Differ Equ Dyn Syst (2012) 20:301–322
DOI 10.1007/s12591-012-0104-z

ORIGINAL RESEARCH

Bifurcational Dynamics of a Two-Dimensional Stick-Slip System

Grzegorz Kudra · Jan Awrejcewicz

Published online: 10 February 2012
© Foundation for Scientific Research and Technological Innovation 2012

Abstract A two degree of freedom plane disk, performing one-dimensional translational and rotational motion, placed on the moving belt, is mathematically modelled and numerically analysed. The friction model for sliding phase is developed assuming classical Coulomb friction law, valid for any infinitesimal element of circular contact area. As a result, the integral expressions for friction force and torque are obtained. The exact integral model is then approximated by the use of different functions, like Padé approximants or their modifications. Some generalizations of the approximate functions used by other authors are proposed. The special event-driven model of the investigated system together with numerical simulation algorithm is developed, where in particular the transition conditions between the stick and slip modes are defined. Some examples of numerical simulation and analysis by the use of Poincaré maps and bifurcational diagrams are presented. It has been shown, that for certain parameter sets, the investigated system exhibits very rich multi-periodic stick-slip oscillations.

Keywords Stick-slip · Event-driven · Coupled friction model · Padé approximants

Introduction

In real mechanical systems, one can very often encounter a situation, when two or more bodies contact directly each other, leading to impact and friction phenomena. In mathematical modelling of such systems, it is common to treat them as working in different modes with the quick transitions between successive phases. Very often the transition from one mode to another is modelled as instantaneous and the system can be described by the use

G. Kudra (✉) · J. Awrejcewicz
Department of Automation and Biomechanics, Technical University of Lodz, Stefanowski 1/15, 90-924 Lodz, Poland
e-mail: grekudra@p.lodz.pl

J. Awrejcewicz
e-mail: awrejcew@p.lodz.pl

of the piecewise smooth differential equations (PWS). Mechanical systems with dry friction are then often modelled as systems possessing discontinuous damping characteristics and belonging to the class of PWS.

Modelling and analysis of friction pair systems exhibiting stick-slip phenomena belongs to a classical problem of nonlinear dynamics but being still developed and attractive for researchers [1–5] because of its importance in real engineering systems. Mainly the classical dimensional Coulomb friction law is assumed in modelling, since it is simple and effective approach to many engineering friction problems. Moreover, the friction process is usually recognized as one-dimensional problem, i.e. when friction force simply opposes relative velocity.

One-dimensional friction model is justified in cases of the very small contact between two bodies (the point contact). Then sliding friction force opposes the sliding relative velocity and can be successfully modelled by the use of classical one-dimensional Coulomb friction law. In this case the friction torque (drilling friction) and its influence on sliding friction force can be neglected (since the contact point cannot transmit a torque). But there are many examples of dynamical behaviour of mechanical systems (billiard ball, Thompson top, wobblestone, electric polishing machine) which cannot be mathematically modelled (in order to obtain correct numerical simulation) or explained assuming one-dimensional dry friction model.

In the work [6], Contensou indicated that relative normal angular velocity (spin) takes place an important role in dynamics of some mechanical systems, where contact between two bodies or spin is relatively large. He developed a two-dimensional mathematical model of friction, based on the classical Coulomb friction law and being a function of two variables: relative sliding velocity of the centre of the non-point circular contact area between two interacting bodies and relative normal angular velocity. He obtained results in the integral and numerical forms for the contact stress distribution according to Hertz theory. A quarter of century later, the results of Contensou were essentially developed by Zhuravlev [7,8], who gave exact analytical expressions for friction force and torque in the case of circular contact as well as corresponding Padé approximations, more convenient to use in practical problems of modelling and simulation. In the next step, a three-dimensional friction model with circular Hertz contact and coupling between friction and rolling resistance, where rolling resistance is a result of a special distortion of contact stress distribution, was developed [9]. Another approach to the problem is presented in work [10], where the coupled friction model for circular contact area with circular symmetry of contact stress distribution (without rolling resistance) was approximated by the use of Taylor expansion of the velocity pseudo potential and then used in the Thompson top modelling and simulation. This problem of coupling between different components of friction is noticed and investigated intensively by scientists recently (see, for instance, a work [11], where the two-dimensional bristle model of friction is developed).

The mathematical modelling and corresponding numerical methods [12] of mechanical systems simulation are two closely related problems. In the case of the mechanical systems with frictional contacts, the numerical simulation techniques can be classified as follows [13]: (a) regularization methods; (b) event driven integration methods; (c) time stepping methods [14,15]. The regularization methods [16] rely on the smoothing of the PWS or differential inclusions systems and result in smooth differential equations allowing for the use of classical integration methods. However, the stiffness of the obtained problem and possibility of loss of some original physical properties of the system belong to some disadvantages of this approach. The event driven integration methods [17–19] use classical integration methods between switches (transition between modes) and (especially for more complex configurations) linear or nonlinear complementarity problem (LCP or NCP) or Augmented Lagrangian

method (ALM) to determine the next mode at each event (the instance of crossing the switching boundary). Time-stepping methods [20–22] are especially developed methods, and they do not require the determination (in contrast to event-driven methods) of the instances of crossing the switching boundary. In this case the LCP, NCP or ALM methods are applied to determine the mode of the system at each the time step.

To the authors' observation there is still a lack or it is difficult to find any work concerned modelling and analysis of stick-slip self-excited vibrations occurring in the system, where there is a coupling between friction force components and friction torque. The aim of this paper is to begin to fill this gap by modelling and numerical simulation of simple two-degree of freedom mechanical system with two-dimensional dry friction phenomenon. The paper is organised as follows. Firstly the model scheme of the mechanical system under investigation is presented together with corresponding differential governing equations in non-dimensional form. In the next section the coupled friction model based on the classical friction law for an infinitesimal element in the integral form is introduced along with different approximate models. Many of that approximants base on approximations earlier proposed by some authors [7–9,23], however here we try to generalize some of the results. Then the event-driven hybrid dynamical model of the investigated system along with the special algorithm for its numerical simulation, is introduced. In the next step, some examples of numerical analysis of the system exhibiting complicated periodic dynamics are presented.

Mechanical System

In Fig. 1 a mechanical system is presented, where two-dimensional coupled dry friction phenomenon occurs and where a self-excited oscillations induced by a two-dimensional stick-slip phenomenon can also be found. The presented system can be also used for investigations on possibility of occurrence of self-excited oscillations induced by the coupling of friction force and torque (independently of a stick-slip phenomenon). The fundamental part of the system is a plane disk of radius $\hat{r}$, mass $\hat{m}$ and moment of inertia $\hat{B}$ (with respect to the axis perpendicular to the disk plane and containing the geometrical centre of the disk being simultaneously the mass centre of the disk) imposed on a moving belt of velocity $\hat{v}_b$. Between the disk and the belt dry friction occurs, which mathematical model will be introduced in the next section. The disk is joined with elasto-damping elements of stiffness $1/2\hat{k}_1$ and $1/2\hat{k}_2$ and with viscous damping coefficients $1/2\hat{c}_1$ and $1/2\hat{c}_2$, respectively. The joining is made by the use of two or four separate cords winding the disk in a way shown in the figure. The cords are tight all the time during the motion of the disk by appropriate initial tension of the springs. The position of the disk is described by the following two coordinates: $\hat{x}$ defining the linear position of the geometrical (mass) centre of the disk along the belt axis and angular φ. Moreover, we assume that the disk does not move along direction perpendicular to the belt axis and an additional external forcing $\hat{F}$ at the disk centre is applied.

The governing differential equations of the system have the following form

$$\begin{aligned} &\hat{m}\hat{x}'' + \hat{k}_1\left(\hat{x} - \varphi\hat{r}\right) + \hat{k}_2\left(\hat{x} + \varphi\hat{r}\right) + \hat{c}_1\left(\hat{x}' - \varphi'\hat{r}\right) + \hat{c}_2\left(\hat{x}' + \varphi'\hat{r}\right) + \hat{T} = \hat{F}\left(\hat{t}\right), \quad (1)\\ &\hat{B}\varphi'' - \hat{k}_1\left(\hat{x} - \varphi\hat{r}\right)\hat{r} + \hat{k}_2\left(\hat{x} + \varphi\hat{r}\right)\hat{r} - \hat{c}_1\left(\hat{x}' - \varphi'\hat{r}\right)\hat{r} + \hat{c}_2\left(\hat{x}' + \varphi'\hat{r}\right)\hat{r} + \hat{M} = 0, \end{aligned}$$

where $\hat{T}$ and $\hat{M}$ are dry friction force and torque, respectively, and $(\ldots)'$ denotes the derivative with respect to real time $\hat{t}$.

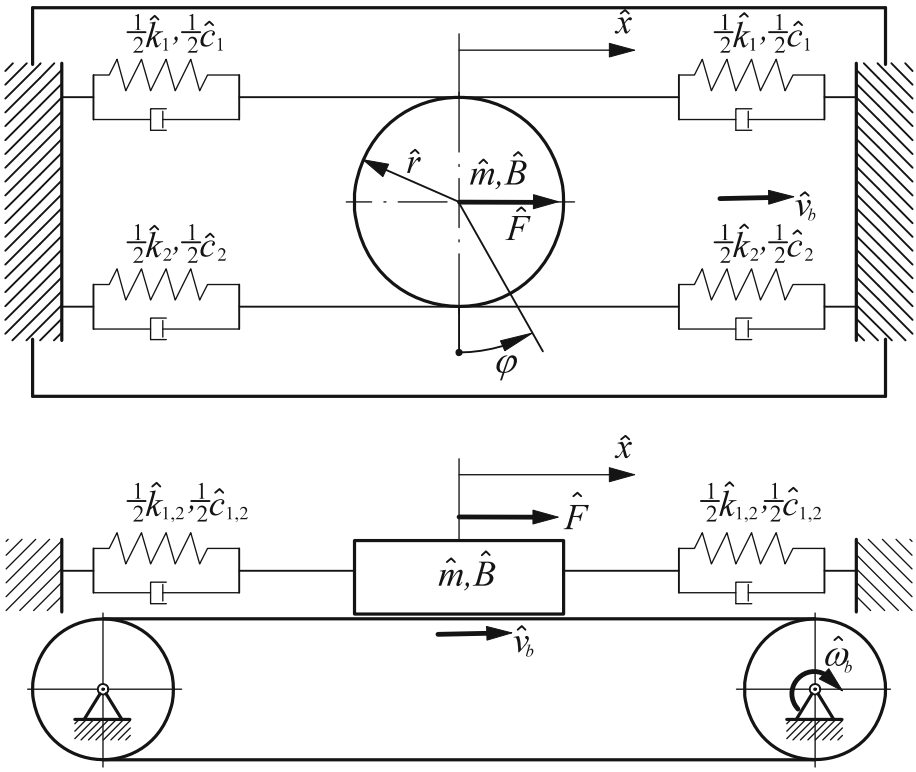

Fig. 1 The mechanical system under investigation

Introducing the following non-dimensional quantities

$$x = \frac{\hat{x}}{\hat{r}},\ t = \alpha \hat{t}, \quad \text{where} \quad \alpha = \sqrt{\frac{\hat{k}_1 + \hat{k}_2}{\hat{m}}}, \tag{2}$$

we get the following non-dimensional matrix form of the governing equations

$$\mathbf{M}\ddot{\mathbf{q}} + \mathbf{C}\dot{\mathbf{q}} + \mathbf{K}\mathbf{q} + \mathbf{F}_T\left(\mathbf{q}, \dot{\mathbf{q}}, t\right) = \mathbf{F}_e\left(t\right), \tag{3}$$

where $\dot{(\ldots)}$ denotes the derivative with respect to real time t and where the following notation has been introduced

$$\mathbf{q} = \begin{Bmatrix} x \\ \varphi \end{Bmatrix}, \quad \mathbf{M} = \begin{bmatrix} 1 & 0 \\ 0 & m \end{bmatrix}, \quad \mathbf{K} = \begin{bmatrix} 1 & k_{12} \\ k_{12} & 1 \end{bmatrix}, \mathbf{C} = \begin{bmatrix} c & c_{12} \\ c_{12} & c \end{bmatrix},$$
$$\mathbf{F}_T\left(\mathbf{q}, \dot{\mathbf{q}}, t\right) = \begin{Bmatrix} T \\ M \end{Bmatrix}, \quad \mathbf{F}_e\left(t\right) = \begin{Bmatrix} F\left(t\right) \\ 0 \end{Bmatrix}.$$

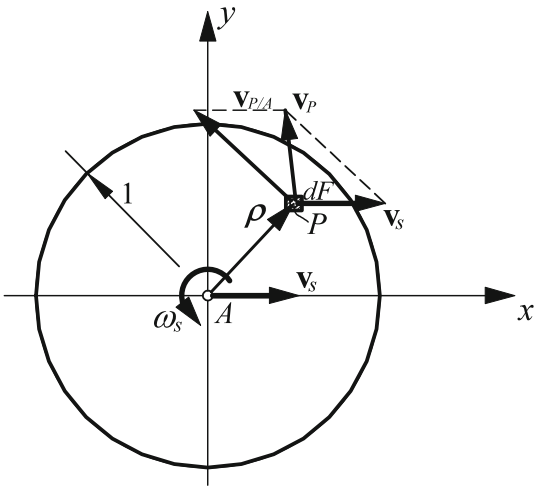

Fig. 2 The contact area of the disk and belt

The relations between real and non-dimensional parameters and forces are as follows

$$m = \frac{\hat{B}}{\hat{m}\hat{r}^2}, \quad k_{12} = \frac{\hat{k}_2 - \hat{k}_1}{\hat{k}_1 + \hat{k}_2}, \quad c = \frac{\hat{c}_1 + \hat{c}_2}{\sqrt{\hat{m}(\hat{k}_1 + \hat{k}_2)}}, \quad c_{12} = \frac{\hat{c}_2 - \hat{c}_1}{\sqrt{\hat{m}(\hat{k}_1 + \hat{k}_2)}},$$
$$T = \frac{\hat{T}}{\hat{r}(\hat{k}_1 + \hat{k}_2)}, \quad M = \frac{\hat{M}}{\hat{r}^2(\hat{k}_1 + \hat{k}_2)}, \quad F = \frac{\hat{F}}{\hat{r}(\hat{k}_1 + \hat{k}_2)}, \tag{4}$$
$$v_b = \frac{\hat{v}_b}{\alpha\hat{r}},$$

where v_b is non-dimensional velocity of the belt.

Friction Model

Let us consider the presented in Fig. 2 non-dimensional circular contact between two bodies of area F. The relative motion of the contact area is described by the use of non-dimensional velocity $\mathbf{v}_s$ of the pole A (centre of the contact) and non-dimensional angular velocity $\boldsymbol{\omega}_s$. We introduce the coordinate system $Axyz$, where axes x and y lie in the contact plane and the x axis has direction of the velocity $\mathbf{v}_s$. The quantities used to describe the model of friction refer to the dimensionless length related to characteristic real dimension $\hat{r}$, therefore dimensionless coordinates of the element dF (the point P) position are $x = \hat{x}/\hat{r}$ and $y = \hat{y}/\hat{r}$, where $\hat{x}$ and $\hat{y}$ are the corresponding real coordinates whereas dimensionless element of area equals $dF = d\hat{F}/\hat{r}^2$, where $d\hat{F}$ is the real element. A consequence of dimensionless length and time is the dimensionless velocity $\mathbf{v}_s = \hat{\mathbf{v}}_s/(\alpha\hat{r})$ and $\boldsymbol{\omega}_s = \hat{\boldsymbol{\omega}}_s/\alpha$, where $\hat{\mathbf{v}}_s$ is real velocity of the point A, $\hat{\boldsymbol{\omega}}_s$ is real angular velocity of the contact area and where the relation between non-dimensional t and real time $\hat{t}$ is $t = \alpha\hat{t}$.

Assuming that the classical Coulomb friction law is valid on each element dF with non-dimensional velocity $\mathbf{v}_P = \hat{\mathbf{v}}_P/(\alpha\hat{r})$ (where $\hat{\mathbf{v}}_P$ is real velocity of the point P), we obtain the following dimensionless form of corresponding infinitesimal dry friction force $d\mathbf{T}_s = d\hat{\mathbf{T}}_s/(\mu\hat{N})$(where $d\hat{\mathbf{T}}_s$ is the corresponding real force, $\hat{N}$ is the normal component of resultant real force of interaction between bodies and μ is dry friction coefficient) acting on the

body lying above the area F and the corresponding dimensionless infinitesimal moment of dry friction force $d\mathbf{M}_s = d\hat{\mathbf{M}}_s/(\hat{r}\mu\hat{N})$ (where $d\hat{\mathbf{M}}_s$ is its real counterpart) with respect to the pole A

$$d\mathbf{T}_s = -\sigma\,(x,\,y)\,\frac{\mathbf{v}_P}{\|\mathbf{v}_P\|}dF, \quad d\mathbf{M}_s = \boldsymbol{\rho}\times d\mathbf{T}_s \tag{5}$$

where dimensionless normal stress distribution $\sigma(x,\,y) = \hat{\sigma}\,(x,\,y)\hat{r}^2/\hat{N}$ has been introduced (where $\hat{\sigma}\,(x,\,y)$ is the real stress distribution), whereas $\boldsymbol{\rho} = \hat{\boldsymbol{\rho}}/\hat{r} = \overrightarrow{AP}$ is dimensionless vector coupling the pole A with the element dF (where $\hat{\boldsymbol{\rho}}$ is its real counterpart). One can easily find that the nondimensional relation (5) is equivalent to the dimensional differential form of the Coulomb friction law for an element $d\hat{F}$: $d\hat{\mathbf{T}}_s = -\mu\hat{\sigma}\,(x,\,y)\,d\hat{F}\hat{\mathbf{v}}_P/\|\hat{\mathbf{v}}_P\|$ and $d\hat{\mathbf{M}}_s = \hat{\boldsymbol{\rho}}\times d\hat{\mathbf{T}}_s$.

The resultant dimensionless friction force and dimensionless friction torque are as follows

$$\mathbf{T}_s = -\int\!\!\int_F \sigma\,(x,\,y)\frac{\mathbf{v}_P}{\|\mathbf{v}_P\|}dF, \quad \mathbf{M}_s = -\int\!\!\int_F \sigma\,(x,\,y)\frac{\boldsymbol{\rho}\times\mathbf{v}_P}{\|\mathbf{v}_P\|}dF \tag{6}$$

Taking into consideration that $\mathbf{v}_P = \mathbf{v}_s + \boldsymbol{\omega}_s\times\boldsymbol{\rho}$, where $\boldsymbol{\omega}_s\times\boldsymbol{\rho} = \mathbf{v}_{P/A}$, we obtain the following relations

$$\begin{aligned}\mathbf{v}_P &= v_{Px}\mathbf{e}_x + v_{Py}\mathbf{e}_y = (v_s - \omega_s y)\,\mathbf{e}_x + \omega_s x\mathbf{e}_y,\\ \boldsymbol{\rho}\times\mathbf{v}_P &= \left(xv_{Px} - yv_{Py}\right)\mathbf{e}_z = \left(\omega_s\left(x^2+y^2\right) - v_s y\right)\mathbf{e}_z,\end{aligned} \tag{7}$$

where $\mathbf{e}_x$, $\mathbf{e}_y$ and $\mathbf{e}_z$ are the unit vectors of the corresponding axes. Now the corresponding components of the friction model can be expressed as follows

$$\begin{aligned}T_{sx}\,(v_s,\omega_s) &= \int\!\!\int_F \sigma\,(x,\,y)\,\frac{v_s - \omega_s y}{\sqrt{(v_s-\omega_s y)^2 + \omega_s^2 x^2}}dxdy,\\ T_{sy}\,(v_s,\omega_s) &= \int\!\!\int_F \sigma\,(x,\,y)\,\frac{\omega_s x}{\sqrt{(v_s-\omega_s y)^2 + \omega_s^2 x^2}}dxdy,\\ M_s\,(v_s,\omega_s) &= \int\!\!\int_F \sigma\,(x,\,y)\,\frac{\omega_s\left(x^2+y^2\right) - v_s y}{\sqrt{(v_s-\omega_s y)^2 + \omega_s^2 x^2}}dxdy,\end{aligned} \tag{8}$$

where the signs has been changed in order to simplify the notation. It means that the friction force and torque are $\mathbf{T}_s = -T_{sx}\mathbf{e}_x - T_{sy}\mathbf{e}_y$ and $\mathbf{M}_s = -M_s\mathbf{e}_z$.

Assuming

$$v_s = \lambda_s\cos\theta_s, \quad \omega_s = \lambda_s\sin\theta_s, \quad \text{where}\,\lambda_s = \sqrt{v_s^2+\omega_s^2} \tag{9}$$

from (8) we obtain the following form of the friction components as functions of one variable θ_s

$$\begin{aligned} T_{sx}(\theta_s) &= \int\int_F \sigma(x,y)\frac{\cos\theta_s - \sin\theta_s y}{\sqrt{(\cos\theta_s - \sin\theta_s y)^2 + \sin^2\theta_s x^2}}dxdy, \\ T_{sy}(\theta_s) &= \int\int_F \sigma(x,y)\frac{\sin\theta_s x}{\sqrt{(\cos\theta_s - \sin\theta_s y)^2 + \sin^2\theta_s x^2}}dxdy, \\ M_s(\theta_s) &= \int\int_F \sigma(x,y)\frac{\sin\theta_s\left(x^2+y^2\right) - \cos\theta_s y}{\sqrt{(\cos\theta_s - \sin\theta_s y)^2 + \sin^2\theta_s x^2}}dxdy. \end{aligned} \tag{10}$$

In further considerations we assume uniform normal stress distribution of the following non-dimensional form

$$\sigma(x,y) = \frac{\hat{\sigma}(x,y)\hat{r}^2}{\hat{N}} = \frac{1}{\pi}, \tag{11}$$

where $\hat{\sigma}(x,y) = \hat{N}/(\pi\hat{r}^2)$. Introducing (11) to Eq. 8 we obtain

$$\begin{aligned} T_{sx}(v_s,\omega_s) &= \frac{1}{\pi}\int\int_F \frac{v_s - \omega_s y}{\sqrt{(v_s-\omega_s y)^2 + \omega_s^2 x^2}}dxdy, \\ M_s(v_s,\omega_s) &= \frac{1}{\pi}\int\int_F \frac{\omega_s\left(x^2+y^2\right) - v_s y}{\sqrt{(v_s-\omega_s y)^2 + \omega_s^2 x^2}}dxdy, \end{aligned} \tag{12}$$

and one can easily find that $T_{sy}(v_s,\omega_s) = 0$. Then introducing the polar coordinate system (ρ,ϕ) such that $x = \rho\cos\phi$ and $y = \rho\sin\phi$ we get from (12) the following form of integral friction model

$$\begin{aligned} T_{sx}(v_s,\omega_s) &= \frac{1}{\pi}\int_0^{2\pi}\int_0^1 \frac{v_s - \rho\omega_s\sin\phi}{\sqrt{v_s^2 + \rho^2\omega_s^2 - 2\rho v_s\omega_s\sin\phi}}\rho d\rho d\phi, \\ M_s(v_s,\omega_s) &= \frac{1}{\pi}\int_0^{2\pi}\int_0^1 \frac{\rho\omega_s - v_s\sin\phi}{\sqrt{v_s^2 + \rho^2\omega_s^2 - 2\rho v_s\omega_s\sin\phi}}\rho^2 d\rho d\phi. \end{aligned} \tag{13}$$

Exact integral forms (13) of the friction model are inconvenient for direct use in mathematical modelling and numerical simulations (very time consuming numerical integration over the F area). The exact analytical solutions to the above integrals exist but they are rather complex [7–10]. In order to obtain relatively simple friction models but preserving essential properties of the full integral expressions (13), one can try to construct special approximants.

$$\begin{aligned} &T_{sx}|_{v_s=0} = 0, \quad T_{sx}|_{\omega_s=0} = \frac{v_s}{|v_s|}, \quad M_s|_{v_s=0} = \frac{2}{3}\frac{\omega_s}{|\omega_s|}, \quad M_s|_{\omega_s=0} = 0, \\ &\left.\frac{\partial T_{sx}}{\partial v_s}\right|_{v_s=0} = \frac{1}{|\omega_s|}, \quad \left.\frac{\partial T_{sx}}{\partial \omega_s}\right|_{\omega_s=0} = 0, \quad \left.\frac{\partial M_s}{\partial v_s}\right|_{v_s=0} = 0, \quad \left.\frac{\partial M_s}{\partial \omega_s}\right|_{\omega_s=0} = \frac{1}{4}\frac{1}{|v_s|}, \\ &\left.\frac{\partial^2 T_{sx}}{\partial \omega_s^2}\right|_{\omega_s=0} = -\frac{1}{4}\frac{1}{v_s|v_s|}, \quad \left.\frac{\partial^2 M_s}{\partial v_s^2}\right|_{v_s=0} = -\frac{1}{\omega_s|\omega_s|}. \end{aligned} \tag{14}$$

Let as try to assume the following form of bivariate Padé approximant [24,25] of the f component of the friction model

$$f^{(P_n)}(v_s,\omega_s)=\frac{\sum_{i=0}^{n}a_{f_x,i}v_s^i\omega_s^{n-i}}{\sum_{i=0}^{n}b_{f_x,i}v_s^i\omega_s^{n-i}},\quad f=T_{sx},M_s, \tag{15}$$

where $b_{f,0}=1$, $a_{f,i}=a_{f,i}(\mathrm{sgn}(v_s),\mathrm{sgn}(\omega_s))$ and $b_{f,i}=b_{f,i}(\mathrm{sgn}(v_s),\mathrm{sgn}(\omega_s))$. The above form of approximation can be understood as a generalization of all the approximate models of friction for circular contact area with Hertz stress distribution presented in certain series of works [7–9].

Assuming $u=v_s/\omega_s$, we get the following form of (15)

$$f^{(P_n)}(v_s,\omega_s)=\frac{\sum_{i=0}^{n}a_{f_x,i}u^i}{\sum_{i=0}^{n}b_{f_x,i}u^i},\quad f=T_{sx},M_s, \tag{16}$$

which can be understood as a univariate two-point (since it fulfills certain derivatives of the integral model at two points: $u=0$ and $\left|u^{-1}\right|=0$) and diagonal Padé approximation. The expression (15) can be also written as follows

$$f^{(P_n)}(\theta_s)=\frac{\sum_{i=0}^{n}a_{f_x,i}\cos^i\theta_s\sin^{n-i}\theta_s}{\sum_{i=0}^{n}b_{f_x,i}\cos^i\theta_s\sin^{n-i}\theta_s},\quad f=T_{sx},M_s, \tag{17}$$

where the relations (9) have been used.

For $n=1$ from (15) we get the following form of approximation

$$f^{(P_1)}(v_s,\omega_s)=\frac{a_{f,0}\omega_s+a_{f,1}v_s}{\omega_s+b_{f,1}v_s},\quad f=T_{sx},M_s. \tag{18}$$

From the following conditions and making use of Eq. 14

$$\begin{aligned}
&T_{sx}|_{v_s=0}=T_{sx}^{(P_1)}\Big|_{v_s\to0^{\pm}},\quad T_{sx}|_{\omega_s=0}=T_{sx}^{(P_1)}\Big|_{\omega_s\to0^{\pm}},\quad \frac{\partial T_{sx}}{\partial v_s}\Big|_{v_s=0}=\frac{\partial T_{sx}^{(P_1)}}{\partial v_s}\Big|_{v_s\to0^{\pm}},\\
&M_s|_{v_s=0}=M_s^{(P_1)}\Big|_{v_s\to0^{\pm}},\quad M_s|_{\omega_s=0}=M_s^{(P_1)}\Big|_{\omega_s\to0^{\pm}},\quad \frac{\partial M_s}{\partial \omega_s}\Big|_{\omega_s=0}=\frac{\partial M_s^{(P_1)}}{\partial \omega_s}\Big|_{\omega_s\to0^{\pm}},
\end{aligned} \tag{19}$$

we get the set of coefficients

$$\begin{aligned}
&a_{T_{sx},0}=0,\quad a_{T_{sx},1}=\mathrm{sgn}(\omega_s),\quad b_{T_{sx},1}=\mathrm{sgn}(\omega_s)\,\mathrm{sgn}(v_s),\\
&a_{M_s,0}=\frac{2}{3}\mathrm{sgn}(\omega_s),\quad a_{M_s,1}=0,\quad b_{M_s,1}=\frac{8}{3}\mathrm{sgn}(\omega_s)\,\mathrm{sgn}(v_s).
\end{aligned} \tag{20}$$

Finally we obtain the following approximation

$$T_{sx}^{(P_1)}(v_s,\omega_s)=\frac{v_s}{|v_s|+|\omega_s|},\quad M_s^{(P_1)}(v_s,\omega_s)=\frac{2\omega_s}{3|\omega_s|+8|v_s|}. \tag{21}$$

In a similar way we find the Padé approximation for $n=2$. Fulfilling all the (14) conditions we get

$$T_{sx}^{(P_2)}(v_s,\omega_s)=\frac{8v_s|v_s|+v_s|\omega_s|}{8v_s^2+|v_s\omega_s|+\omega_s^2},\quad M_s^{(P_2)}(v_s,\omega_s)=\frac{64\omega_s|\omega_s|+18\omega_s|v_s|}{96\omega_s^2+27|v_s\omega_s|+72v_s^2}. \tag{22}$$

The comparison of the developed above Padé' approximants (21) and (22) to the corresponding exact integral components (13) computed numerically is presented in Fig. 3, where

the notations $T_{sx}^{(c)} = T_{sx}$ and $M_s^{(c)} = M_s$ have been used. Because all the plotted functions $T_{sx}^{(a)}(\theta_s)$ and $M_s^{(a)}(\theta_s)$ (where a is a kind of approximation) possesse, the corresponding properties of the functions sine and cosine correspondingly, allowing to compute the value of the function for an arbitrary φ_s knowing its values for $\theta_s \in [0, \pi/2]$, the plots $T_{sx}^{(a)}(\theta_s)$ and $M_s^{(a)}(\theta_s)$ are made for the first quarter only. Observing the plots one can find that 2nd order approximation is more accurate than a 1st order one.

The similarity of the parametric plot of full integral model presented in Fig. 3 to the ellipse [23], can suggest the another approximation of the following form

$$T_{sx}^{(I)}(\theta_s) = \cos\theta_s, \quad M_s^{(I)}(\theta_s) = \frac{2}{3}\sin\theta_s, \tag{23}$$

or

$$T_{sx}^{(I)}(v_s, \omega_s) = \frac{v_s}{\sqrt{v_s^2 + \omega_s^2}}, \quad M_s^{(I)}(v_s, \omega_s) = \frac{2\omega_s}{3\sqrt{v_s^2 + \omega_s^2}}. \tag{24}$$

The comparison of the approximants (23) to the exact integral model and the corresponding absolute errors are presented in Fig. 3. One can observe that the model (23) is approximately of the same accuracy (in the sense of absolute errors) as the Padé approximation for $n = 2$ (22). Note, that simultaneously the model (23) is much more simple than the approximants (22). Moreover, the parametric plot exhibited by Fig. 3a indicates the greater suitability of the approximations $T_{sx}^{(I)}$ and $M_s^{(I)}$. One can also notice (see Fig. 3b, c) that the corresponding first derivatives of the $M_s^{(I)}(\theta_s)$ component are not satisfied at the points $\theta_s = k\pi$, where $k \in \mathrm{C}$.

One can try to generalize the approximation (24) in the following way

$$f^{(I_n)}(v_s, \omega_s) = \frac{\sum_{i=0}^{n} a_{f,i} v_s^i \omega_s^{n-i}}{\sqrt{\sum_{i=0}^{2n} b_{f,i} v_s^i \omega_s^{2n-i}}}, \quad f = T_{sx}, M_s, \tag{25}$$

or using the equivalent form

$$f^{(I_n)}(\theta_s) = \frac{\sum_{i=0}^{n} a_{f,i} \cos^i\theta_s \sin^{n-i}\theta_s}{\sqrt{\sum_{i=0}^{2n} b_{f,i} \cos^i\theta_s \sin^{2n-i}\theta_s}}, \quad f = T_{sx}, M_s, \tag{26}$$

where $b_{fx,0} = 1$.

In order to obtain the approximation (24) we take $n = 1$, then assume $b_{f,1} = 0$ and $b_{f,2} = 1$. The remaining coefficients of the approximation $f^{(I_1)}$ are found from the conditions $f|_{v_s=0} = f^{(I_1)}\big|_{v_s=0}$ and $f|_{\omega_s=0} = f^{(I_1)}\big|_{\omega_s=0}$ (where $f = T_{sx}, M_s$). Then we obtain the special case $f^{(I)}$ of the approximation $f^{(I_1)}$.

The coefficients of the full $f^{(I_1)}$ model can be found from the following conditions

$$\begin{aligned} &f|_{v_s=0} = f^{(I)}\Big|_{v_s=0}, \quad f|_{\omega_s=0} = f^{(I)}\Big|_{\omega_s=0}, \\ &\frac{\partial f}{\partial v_s}\bigg|_{v_s=0} = \frac{\partial f^{(I)}}{\partial v_s}\bigg|_{v_s=0}, \frac{\partial f}{\partial \omega_s}\bigg|_{\omega_s=0} = \frac{\partial f^{(I)}}{\partial \omega_s}\bigg|_{\omega_s=0}, \quad f = T_{sx}, M_s, \end{aligned} \tag{27}$$

leading to the following form of approximation

$$T_{sx}^{(I_1)}(v_s, \omega_s) = \frac{v_s}{\sqrt{v_s^2 + \omega_s^2}}, \quad M_s^{(I_1)}(v_s, \omega_s) = \frac{2\omega_s}{\sqrt{64v_s^2 + 9\omega_s^2}}. \tag{28}$$

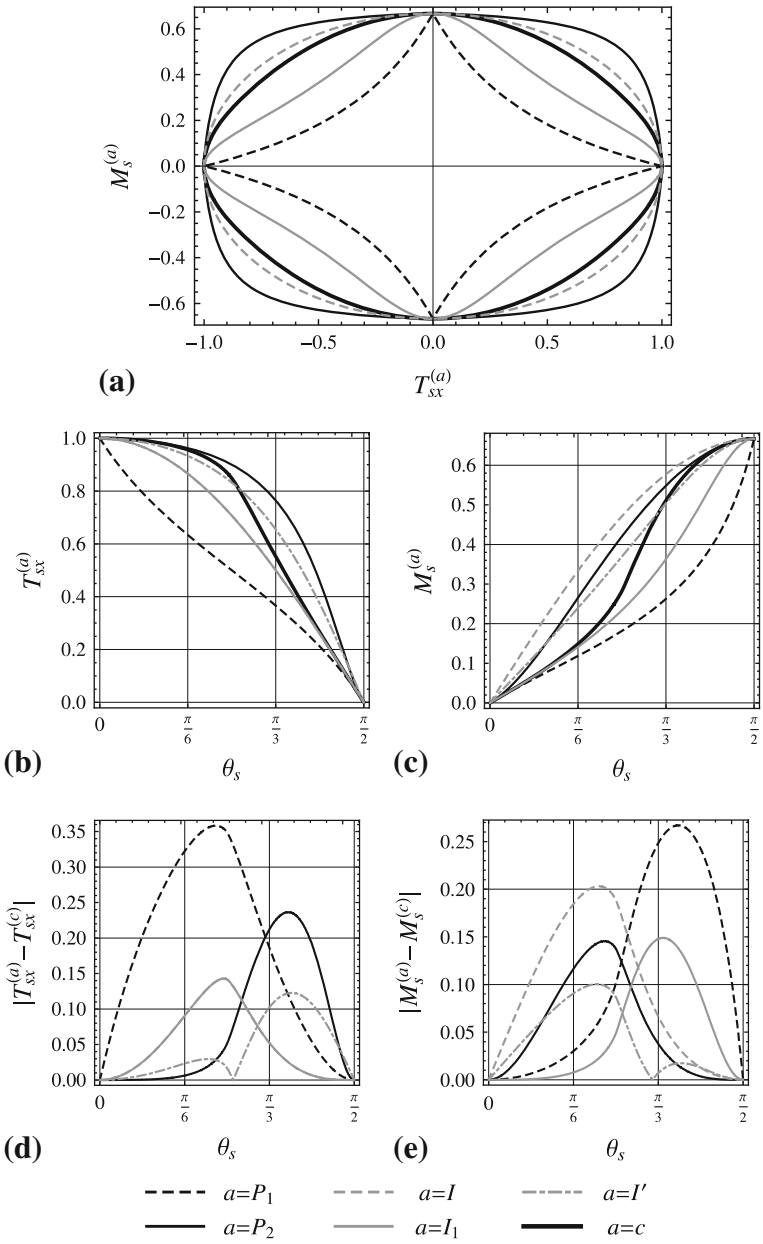

Fig. 3 The comparison of the corresponding approximants to the exact integral model of the friction. The *grey dashed line* in (**b**) and (**d**) is covered by the continuous one

The comparison of the model (28) to the exact integral model and the corresponding absolute errors exhibited by Fig. 3, show that model $T_{sx}^{(I_1)}$ and $M_s^{(I_1)}$ is approximately of the same accuracy (in the sense of absolute errors) as the simpler model $T_{sx}^{(I)}$ and $M_s^{(I)}$. Moreover the approximation $T_{sx}^{(I)}$ and $M_s^{(I)}$ presents itself more advantageously in the parametric plot shown in Fig. 3a.

On the other hand one can easily find the following property of the integral model (10)

$$\frac{dT_{sx}}{d\theta_s} = -\frac{dM_s}{d\theta_s}\tan\theta_s, \tag{29}$$

which means that $dM_s/dT_{sx} = -\cot\theta_s$ and the direction of the generalized velocity of the contact patch $\boldsymbol{\lambda}_s = v_s\mathbf{e}_x + \omega_s\mathbf{e}_z$ is normal to the curve described parametrically by $T_{sx}(\theta_s)$ and $M_s(\theta_s)$. In order to make a use of the above relation while developing the corresponding approximate models, one can try to assume certain form of one of the components ($T_{sx}^{(a)}$ or $M_s^{(a)}$) and then calculate the second component by integration of Eq. 29. But in general, it may occur difficult to find relatively simple forms of both components $T_{sx}^{(a)}$ and $M_s^{(a)}$ satisfying the relation (29).

As a second way to fulfil the property (29), one can try to assume initially the approximate model as two independent components $T_{sx}^{(a)}\left(\theta_s'\right)$ and $M_s^{(a)}\left(\theta_s'\right)$ and then to find the corresponding coefficients assuming $\theta_s' = \theta_s$ and satisfying, for example, some of the conditions (14). In the next stage one can re-parameterize the model by the use of suitable function $\theta_s' = \theta_s'(\theta_s)$ in order to meet the relation (29), however simultaneously loosing the initial fulfillment of the certain conditions. Applying the new parameterization, we get the model $T_{sx}^{(a')}(\theta_s) = T_{sx}^{(a)}\left(\theta_s'(\theta_s)\right)$ and $M_s^{(a')}(\theta_s) = M_s^{(a)}\left(\theta_s'(\theta_s)\right)$. Differentiating the functions $T_{sx}^{(a)}\left(\theta_s'(\theta_s)\right)$ and $M_s^{(a)}\left(\theta_s'(\theta_s)\right)$ with respect to θ_s and making a use of the relation (28) we get

$$\frac{dT_{sx}^{(a)}\left(\theta_s'\right)}{d\theta_s'} = -\frac{dM_s^{(a)}\left(\theta_s'\right)}{d\theta_s'}\tan\theta_s. \tag{30}$$

From the above equation we can find $\theta_s' = \theta_s'(\theta_s)$ at least numerically for general case.

Trying to parameterize once again the model (23) we assume $T_{sx}^{(I)}\left(\theta_s'\right) = \cos\theta_s'$ and $M_s^{(I)}\left(\theta_s'\right) = 2/3\sin\theta_s'$ and then from relation (30) for $a = I$ we obtain

$$\tan\left(\theta_s'\right) = \frac{2}{3}\tan\left(\theta_s\right), \tag{31}$$

which finally (assuming $\operatorname{sgn}(\cos\theta_s') = \operatorname{sgn}(\cos\theta_s)$) leads to the following form of the approximate model [23]

$$T_{sx}^{(I')}(\theta_s) = \frac{\cos\theta_s}{\sqrt{\cos^2\theta_s + \frac{4}{9}\sin^2\theta_s}}, \quad M_s^{(I')}(\theta_s) = \frac{\frac{4}{9}\sin\theta_s}{\sqrt{\cos^2\theta_s + \frac{4}{9}\sin^2\theta_s}}, \tag{32}$$

or

$$T_{sx}^{(I')}(v_s,\omega_s) = \frac{v_s}{\sqrt{v_s^2 + \frac{4}{9}\omega_s^2}}, \quad M_s^{(I')}(v_s,\omega_s) = \frac{\frac{4}{9}\omega_s}{\sqrt{v_s^2 + \frac{4}{9}\omega_s^2}}. \tag{33}$$

The above assumption of $\operatorname{sgn}(\cos\theta_s') = \operatorname{sgn}(\cos\theta_s)$ is motivated by the fact that the reparameterization $\theta_s' = \theta_s'(\theta_s)$ should not change the model of friction too much (in order words the function $\theta_s' = \theta_s'(\theta_s)$ should not differ too much from the function $\theta_s' = \theta_s$). Let us also note, that the assumption of $\operatorname{sgn}(\cos\theta_s') = -\operatorname{sgn}(\cos\theta_s)$ leads to $T_{sx}^{(I')}(v_s,\omega_s) = -v_s/\sqrt{v_s^2 + \frac{4}{9}\omega_s^2}$, which has no sense (for $\omega_s = 0$ the friction force do not oppose the relative velocity).

Comparing the model (32) to the other approximations and exact integral model presented in Fig. 3 (the parametric plot of $\left(T_{sx}^{(I')}, M_s^{(I')}\right)$ as the same plot as $\left(T_{sx}^{(I)}, M_s^{(I)}\right)$ is not shown) we can find that it is the most accurate approximation to the exact integral model, assuming Coulomb friction law and uniform contact pressure distribution. However, in the case of real system modelling, we should expect some uncertainties in both contact pressure distribution and friction law. So it is not obvious which of the approximate models would be most effective in the modelling of real system. One should especially consider the usage of relatively simple model (24).

Now we will try to apply the above developed approximate models to the presented in the previous section mechanical system in the non-dimensional form. Taking into account that $v_s = \alpha^{-1}\hat{r}^{-1}\hat{v}_s$ and $\omega_s = \alpha^{-1}\hat{\omega}_s$ we get

$$v_s = \dot{x} - v_b, \quad \omega_s = \dot{\varphi}, \tag{34}$$

where $\dot{x}$ and $\dot{\varphi}$ are the dimensionless velocities of the disk presented in Fig. 1 while v_b is non-dimensional velocity of the belt.

Assuming that the mechanical system modeled by Eq. 3 is in the sliding phase of motion and taking into account the relations (4) and $\hat{T} = \hat{T}_{sx}^{(a)} = \mu\hat{N}T_{sx}^{(a)}$ together with $\hat{M} = \hat{M}_s^{(a)} = \mu\hat{N}\hat{r}M_s^{(a)}$, we get the following non-dimensional components of the friction model

$$T = \overline{\mu}T_{sx}^{(a)}, \quad M = \overline{\mu}M_s^{(a)}, \tag{35}$$

where

$$\overline{\mu} = \mu\frac{\hat{m}g}{\hat{r}(\hat{k}_1 + \hat{k}_2)} \tag{36}$$

is non-dimensional parameter playing a role of friction coefficient μ and a indicates the kind of approximation used. We assume that $a = c$ denotes the exact integral model, i.e. $T_{sx}^{(c)} = T_{sx}$ and $M_s^{(c)} = M_s$.

Event-Driven Model and Integration Scheme

Let as introduce the discrete variable $i_s(t)$ taking a value of $i_s = 1$ for slip phase of disk motion and a value of $i_s = 0$ during stick phase. Then the friction model can be developed as follows

$$\left\{\begin{array}{l} T\,(x, \dot{x}, \varphi, \dot{\varphi}, i_s, t) \\ M\,(x, \dot{x}, \varphi, \dot{\varphi}, i_s, t) \end{array}\right\} = \left\{\begin{array}{ll} \overline{\mu}\left\{\begin{array}{l} T_{sx}^{(a)}\,(\dot{x} - v_b, \dot{\varphi}) \\ M_s^{(a)}\,(\dot{x} - v_b, \dot{\varphi}) \end{array}\right\} & \text{for } i_s = 1 \\ \overline{\mu}_0\left\{\begin{array}{l} T_{s'x}\,(x, \dot{x}, \varphi, \dot{\varphi}, t) \\ M_{s'}\,(x, \dot{x}, \varphi, \dot{\varphi}, t) \end{array}\right\} & \text{for } i_s = 0 \end{array}\right., \tag{37}$$

where

$$\overline{\mu}_0 = \mu_0\frac{\hat{m}g}{\hat{r}(\hat{k}_1 + \hat{k}_2)}$$

is non-dimensional parameter playing a role of static friction coefficient μ_0. The variables $T_{s'x}$ and $M_{s'}$ are the forces balancing external forces in such a way that the disk move permanently with the belt. Assuming that the disk has acceleration of the belt ($\ddot{x} = 0$ and $\ddot{\varphi} = 0$)

we get

$$\left\{ \begin{array}{c} T_{s'x}\left(x,\dot{x},\varphi,\dot{\varphi},t\right) \\ M_{s'}\left(x,\dot{x},\varphi,\dot{\varphi},t\right) \end{array} \right\} = \frac{1}{\overline{\mu}_0}\left(\left\{ \begin{array}{c} F\left(t\right) \\ 0 \end{array} \right\} - \left[\begin{array}{cc} c & c_{12} \\ c_{12} & c \end{array} \right] \left\{ \begin{array}{c} \dot{x} \\ \dot{\varphi} \end{array} \right\} - \left[\begin{array}{cc} 1 & k_{12} \\ k_{12} & 1 \end{array} \right] \left\{ \begin{array}{c} x \\ \varphi \end{array} \right\} \right). \quad (38)$$

The model should be now supplemented with the rules of transitions between states $i_s = 0$ and $i_s = 1$. The end of the sliding phase is determined by decay of the relative motion of the disk and belt. Since the point $v_s = 0$ and $\omega_s = 0$ for all models developed in the previous section is a singular point, we assume certain threshold value $\varepsilon_{\lambda s} > 0$ such that the sliding phase lasts as long as

$$h_s\left(\dot{x},\dot{\varphi}\right) = \lambda_s\left(\dot{x},\dot{\varphi}\right) - \varepsilon_{\lambda s} = \sqrt{\left(\dot{x} - v_b\right)^2 + \dot{\varphi}^2} - \varepsilon_{\lambda s} \geq 0, \quad (39)$$

where $\lambda_s = \sqrt{v_s^2 + \omega_s^2}$ for v_s and ω_s defined by Eq. 28. After detection of the earliest time instance t_r such that $h_s\left(t\right) < 0$ on the time interval $t \in \left(t_r, t_r + \varepsilon\right)$ for certain $\varepsilon > 0$ (usually falling zero crossing of the $h_s\left(t\right)$ function detection), we perform the small jump of the velocities (in order to improve the accuracy of the simulation) by the use of the following map

$$\left\{ \begin{array}{c} \dot{x}\left(t_r^+\right) \\ \dot{\varphi}\left(t_r^+\right) \end{array} \right\} = \left\{ \begin{array}{c} v_b \\ 0 \end{array} \right\}, \quad (40)$$

where $\dot{x}\left(t_r^+\right)$ and $\dot{\varphi}\left(t_r^+\right)$ are the initial velocities of the next stick phase. Moreover the discrete variable i_s undergoes a change taking a value of 0. The remaining phase variables (displacements) do not change at the time instance t_r.

In order to construct the condition of remaining of the system in the stick phase, we consider the set Ω presented in Fig. 4, whose boundary is defined by the values of friction force and torque in the case of virtual sliding with the static friction coefficient. We say "virtual" since it is a theoretical situation of sliding with friction coefficient equal to its static counterpart. One can also understand it as a limiting state of the sticking phase, when sliding mode begins and its beginning is just understood as "virtual sliding". The boundary of the set Ω is defined parametrically by the suitable models of friction force and torque in the same way as we have plotted the corresponding curves in Fig. 3a (remembering only that the friction coefficient is static even if its non-dimensional value is still equal to one). Trying to generalize one-dimensional case, where the set of admissible values of friction force during the sticking mode is the interval $[-1,1]$ (for non-dimensional case with static friction coefficient equal to one), we conclude that the set Ω is the sticking region (the set of admissible values of friction force $T_{s'x}$ and torque $M_{s'}$ during the sticking mode).

Let us assume the existence of a certain $\xi_{s'}^{(a)} \geqq 0$ such, that $\overline{OS'} = \xi_{s'}^{(a)}\overline{OS}$ where O, S and S' are the points interpreted in Fig. 4. The boundary of the set Ω is determined parametrically by the use of functions $T_{s'x} = T_{sx}^{(a)}\left(\theta_{s'}^{(a)}\right)$ and $M_{s'} = M_s^{(a)}\left(\theta_{s'}^{(a)}\right)$, where a indicates a kind of the approximation used and where we have introduced a new notation $\theta_{s'}^{(a)}$, because now, since we have the sticking phase of motion, the argument of the functions $T_{sx}^{(a)}$ and $M_s^{(a)}$ is not determined from the velocities v_s and ω_s. Then the condition of the lasting of the stick mode is the point S' remaining in the Ω zone, that is $\xi_{s'}^{(a)} \leq 1$. Projecting the equation $\overline{OS'} = \xi_{s'}^{(a)}\overline{OS}$ onto the directions $T_{s'x}$ and $M_{s'}$ correspondingly we get the following scalar equations

$$T_{s'x} = \xi_{s'}^{(a)} T_{sx}^{(a)}\left(\theta_{s'}^{(a)}\right), \quad M_{s'} = \xi_{s'}^{(a)} M_s^{(a)}\left(\theta_{s'}^{(a)}\right), \quad (41)$$

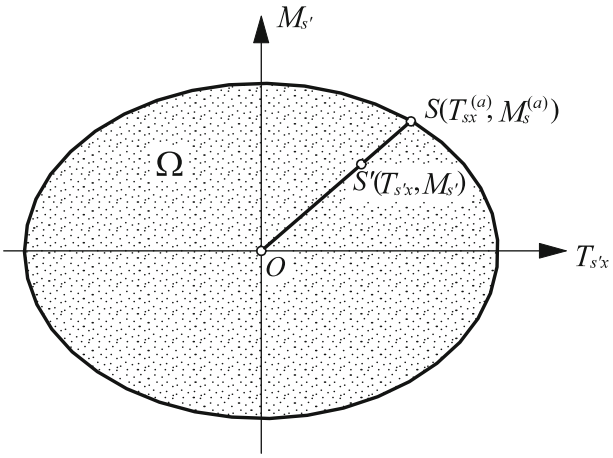

Fig. 4 The geometric interpretation of the point S' in the set of admissible values of the friction model components during the stick phase

from which we can determine $\xi_{s'}^{(a)}$ and $\theta_{s'}^{(a)}$ as functions of $T_{s'x}$ and $M_{s'}$ variables and kind of approximation a. Assuming that the set Ω is convex, the above set of equations (assuming $\xi_{s'}^{(a)} \geqq 0$) has always only one solution. For the zones limited by the approximations presented in Fig. 3, there exists also only one solution, although some of that sets are not convex.

In general, the symbolic solution to the Eq. 41 for the developed in the previous section approximate models may be difficult to find, but one can easily solve them numerically in parallel while integrating numerically the governing equations of motion. In some cases, however, the analytical solution is simple. For example for the approximate model $T_{sx}^{(I)}$ and $M_s^{(I)}$ defined by Eq. 23 we obtain

$$\xi_{s'}^{(I)} = \sqrt{T_{s'x}^2 + \frac{9}{4}M_{s'}^2}, \quad \cos\theta_{s'}^{(I)} = \frac{T_{s'x}}{\xi_{s'}^{(I)}}, \quad \sin\theta_{s'}^{(I)} = \frac{3}{2}\frac{M_{s'}}{\xi_{s'}^{(I)}} \tag{42}$$

For the approximate model $T_{sx}^{(I')}$ and $M_s^{(I')}$ defined by Eq. 31 we get

$$\begin{aligned} \xi_{s'}^{(I')} &= \sqrt{T_{s'x}^2 + \frac{9}{4}M_{s'}^2}, \\ \cos\theta_{s'}^{(I')} &= \frac{T_{s'x}}{\sqrt{T_{s'x}^2 + \frac{81}{16}M_{s'}^2}}, \quad \sin\theta_{s'}^{(I')} = \frac{9}{4}\frac{M_{s'}}{\sqrt{T_{s'x}^2 + \frac{81}{16}M_{s'}^2}}, \end{aligned} \tag{43}$$

where we have assumed, that signs of $\cos\theta_{s'}^{(I')}$ and $T_{sx}^{(I')}$ as well as signs of $\sin\theta_{s'}^{(I')}$ and $M_s^{(I')}$ are the same.

The condition of the stick phase lasting can be described by the following function

$$h_{s'}(x, \dot{x}, \varphi, \dot{\varphi}, t) = 1 - \xi_{s'}^{(a)}(x, \dot{x}, \varphi, \dot{\varphi}, t) \geq 0. \tag{44}$$

The function $\theta_{s'}^{(a)}(x, \dot{x}, \varphi, \dot{\varphi}, t)$ during the stick mode specifies the relation between the linear velocity v_s of the point A and angular velocity ω_s of the contact area during the virtual slip,

which would take place, if the friction coefficient were sufficiently small. Detecting the earliest time instance t_p such that $h_{s'} \geq 0$ on the time interval $t \in \left(t_p, t_p + \varepsilon\right)$ for certain $\varepsilon > 0$ (usually falling zero crossing of the $h_{s'}(t)$ function), we know the direction $\theta_{s'}^{(a)}\left(t_p^-\right)$ (the value of the $\theta_{s'}^{(a)}$ variable at the end instance t_p of the stick phase) of the sliding which would take place, if the friction coefficient were $\overline{\mu}_0$. Assuming that the beginning of the sliding takes place with the friction coefficient $\overline{\mu}_0$, in order to avoid singularities of the approximate models as well as to fulfill the condition $h_s(\dot{x}, \dot{\varphi}) \geq 0$ necessary for the sliding mode, we perform the small jump of the velocities by the use of the following map

$$\begin{Bmatrix} \dot{x}\left(t_p^+\right) \\ \dot{\varphi}\left(t_p^+\right) \end{Bmatrix} = \varepsilon_{\lambda s} \begin{Bmatrix} \cos\theta_{s'}^{(a)}\left(t_p^-\right) \\ \sin\theta_{s'}^{(a)}\left(t_p^-\right) \end{Bmatrix} + \begin{Bmatrix} v_b \\ 0 \end{Bmatrix}, \tag{45}$$

where $\dot{x}\left(t_p^+\right)$ and $\dot{\varphi}\left(t_p^+\right)$ are initial velocities of the next sliding mode. The above equation after taking into account the Eq. 34 fulfills the conditions $v_s\left(t_p^+\right)/\lambda_s\left(t_p^+\right) = \cos\theta_{s'}\left(t_p^-\right)$, $\omega_s\left(t_p^+\right)/\lambda_s\left(t_p^+\right) = \sin\theta_{s'}\left(t_p^-\right)$ and $h_s\left(t_p^+\right) = 0$, where $\lambda_s\left(t_p^+\right) = \varepsilon_{\lambda s}$ and where $v_s\left(t_p^+\right)$, $\omega_s\left(t_p^+\right)$, $h_s\left(t_p^+\right)$ and $\lambda_s\left(t_p^+\right)$ are initial values of the functions v_s, ω_s, h_s and $\lambda_s = \sqrt{v_s^2 + \omega_s^2}$ for the sliding mode at the time instance t_p. In the next step, after the jump of the velocities, the discrete variable i_s takes a value of 0 and the friction coefficient jumps to a new value. The remaining state variables (displacements) are continuous at the time instance t_p.

The above described algorithm is presented in the form of flowchart in Fig. 5. The displacements are continuous at the time instances of transitions between the successive modes. For the integration over the sliding or sticking phases one can use a standard ODEs integration routine, additionally equipped with the corresponding event detection procedure. One of the simplest ones is for example the method of halving the integration step (after detection of the event over a certain time step) until obtaining the required accuracy.

Let us note for a one possible scenario when before beginning of the integration over the stick mode, the value of the function $h_{s'}(t)$ for $t = t_r$ is negative. In such a situation we omit the integration process assuming the final state of the stick phase equal to its initial one. The corresponding jump of velocities following the stick mode can be then understood as the beginning of the sliding process with the friction coefficient large enough (the friction forces are assumed to be on boundary of the set of their admissible values). In the next instance the corresponding change of the friction coefficient takes place before the next integration process. Such an infinitesimal sticking mode can be related to the finite size of the assumed threshold $\varepsilon_{\lambda s}$ determining the transition to the sticking. Taking the smaller value of the $\varepsilon_{\lambda s}$ can cause disappearing of that phenomenon. One can understand it in such a way, that the solution of the sliding mode passes close to singularity $v_s = 0$ and $\omega_s = 0$ but avoids the sticking mode.

Numerical Examples

In the present section we show some examples of numerical simulation and analysis of the above introduced event-driven mechanical system. In all the exhibited examples the following non-dimensional parameters are assumed: $m = 90, k_{12} = 0.85, c = 10^{-4}, c_{12} = 0$, $\overline{\mu} = 5, v_b = 5$ and $F(t) = 0$ (the system without external forcing) while the parameter

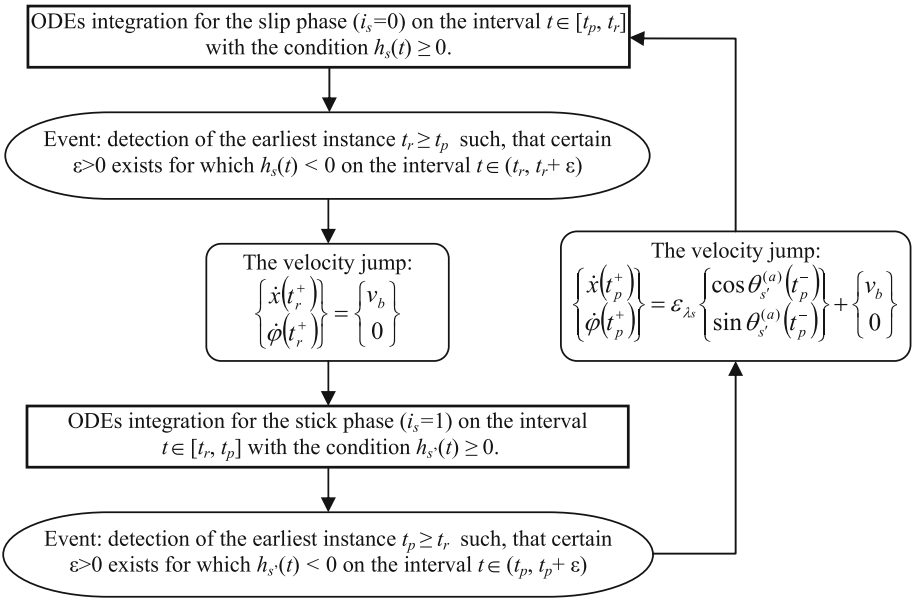

Fig. 5 The flowchart of the numerical integration algorithm

$\overline{\mu}_0$ is varied as a bifurcational one. The threshold of the detection of the singularity is taken as $\varepsilon_{\lambda s} = 10^{-7}$. For the approximation of the exact integral model one of the simplest but effective approximation with components $T_{sx}^{(I)}$ and $M_s^{(I)}$ defined by Eq. 23 is used. For the integration of the differential equations over the slip or stick phases we use the Dormand–Prince method with a relative tolerance of 10^{-10} and an absolute tolerance of 10^{-10}. The presented Poincaré sections and bifurcational diagrams base on the Poincaré map defined as mapping of any initial state of the stick phase to the next initial point of the stick mode.

In Fig. 6 there is shown a bifurcational diagram of the system with the static friction coefficient $\overline{\mu}_0$ varied in the interval [11.2, 25.2]. In Fig. 7 one can see enlargements of two subintervals of the bifurcational diagram from Fig. 6. The first one with $\overline{\mu}_0 \in [11.2, 13.5]$ exhibits the beginning (left-hand side) while the second one with $\overline{\mu}_0 \in [22.5, 25]$ shows the zoom of the end (right-hand side) of the first bifurcational diagram. Although the first look at the fractal-like diagrams may suggest a possibility of existence of irregular attractors, a more deep numerical insight do not prove that. Rather typical for the investigated system is existence of multi-periodic orbits, sometimes of very long periods.

In Figs. 8, 9, 10 one can observe phase plots of three periodic orbits for $\overline{\mu}_0 = 24.9$, $\overline{\mu}_0 = 23.06$ and $\overline{\mu}_0 = 13.5$, respectively. Figure 10 contains also time histories of the corresponding behaviors. The first solution exhibits one point, the second one 3 points while the third one 11 points in the bifurcational diagram and the corresponding Poincaré sections. In Fig. 10 one can notice typical for this system behavior, when from one stick phase to the next one the angular coordinate value decreases until the 11th stick mode after which the angular positions of the disk returns to its initial value.

The corresponding Poincaré sections of the multi-periodic orbits observed in bifurcational diagrams for $\overline{\mu}_0 = 23.0580008$ and $\overline{\mu}_0 = 24.819906$ respectively are shown in Fig. 11. It has been checked the number of points are large but finite. The corresponding phase trajectories are presented in Figs. 12 and 13.

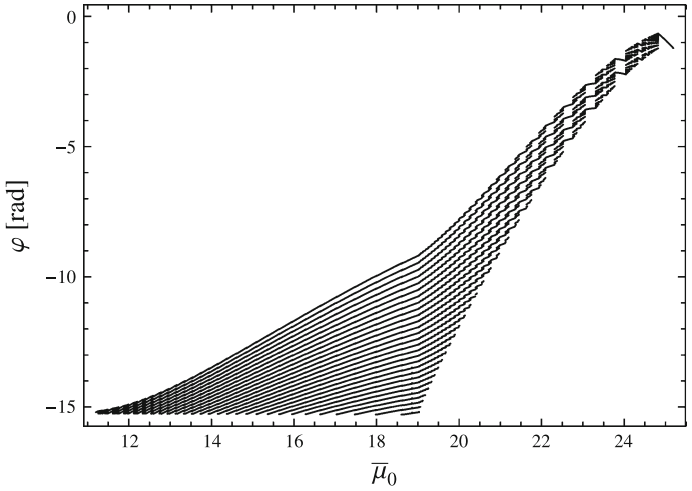

Fig. 6 Bifurcation diagram with static friction coefficient as a control parameter

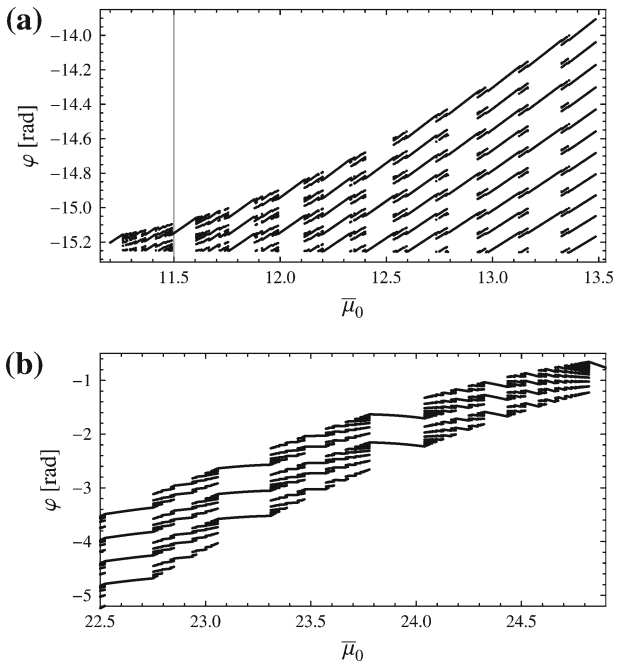

Fig. 7 Enlargements of the bifurcational diagram presented in Fig. 6 on two subintervals of the control parameter

Figure 14 exhibits error Δ of the solution (obtained by the use of Dormand–Prince method with both relative and absolute tolerances of 10^{-10}) as a function of the parameter $\varepsilon_{\lambda s}$. The quantity Δ is defined as maximal deviation between the corresponding solution and the base solution obtained by the use of the same method but with smaller parameter $\varepsilon_{\lambda s} = 10^{-10}$ and smaller relative and absolute tolerances equal to 10^{-13}. The base orbit is a certain

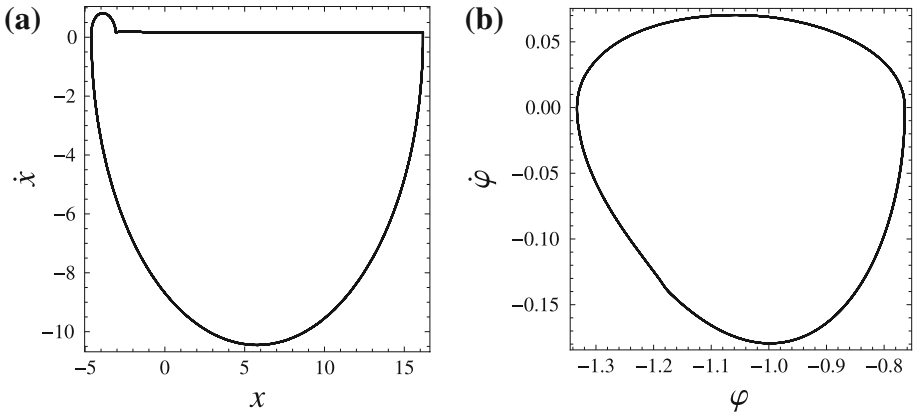

Fig. 8 Periodic orbit for $\overline{\mu}_0 = 24.9$

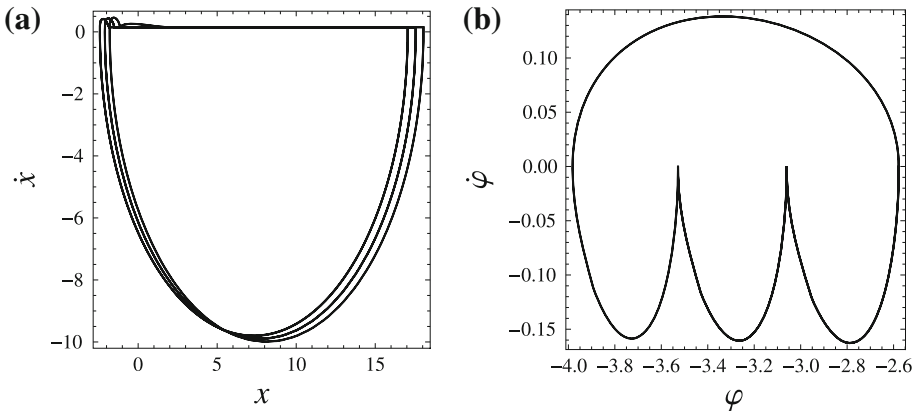

Fig. 9 Periodic orbit for $\overline{\mu}_0 = 23.06$

stable periodic solution while the investigated trajectory starts from a certain point of the base solution. The solutions are then compared on the time interval of the length of 3,000 dimensionless units. Figure 14 exhibits five examples for five different periodic orbits observed for different values of the static friction coefficient $\overline{\mu}_0$ and presented above in Figs. 8, 9, 10, 11, 12, 13, respectively. Initially linear relation between $-\log\Delta$ and $-\log\varepsilon_{\lambda_s}$ (for small ε_{λ_s}) encounters certain threshold and then the investigated solution starts to differ significantly from the base one. That threshold appears, dependently of the case, for relatively high (the solution 1) or small values of the parameter ε_{λ_s} (the solutions 4 and 5). In the cases 4 and 5 it is even smaller (case 5) or approximately equal (case 4) to the value (10^{-7}) of the parameter ε_{λ_s} taken in the regular simulations presented in this paper. It can be explained taking into account possible sensitivity of the system dynamics on parameter changes near different bifurcational phenomena. In order to test the influence of the parameter ε_{λ_s} on the global dynamics of the system, we have additionally computed the bifurcational diagram presented in Fig. 7b for $\varepsilon_{\lambda_s} = 10^{-5}$. The results are exhibited by Fig. 7b, where firstly the bifurcational diagram for $\varepsilon_{\lambda_s} = 10^{-5}$ has been plotted by the use of gray color and then covered by the

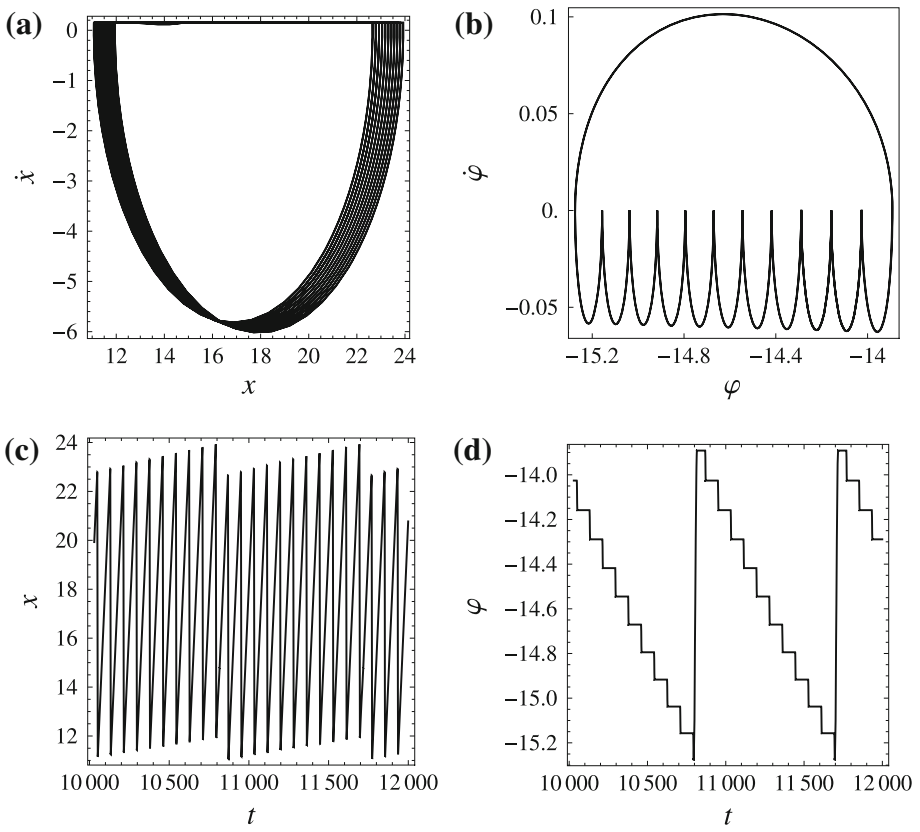

Fig. 10 Periodic orbit for $\overline{\mu}_0 = 13.5$

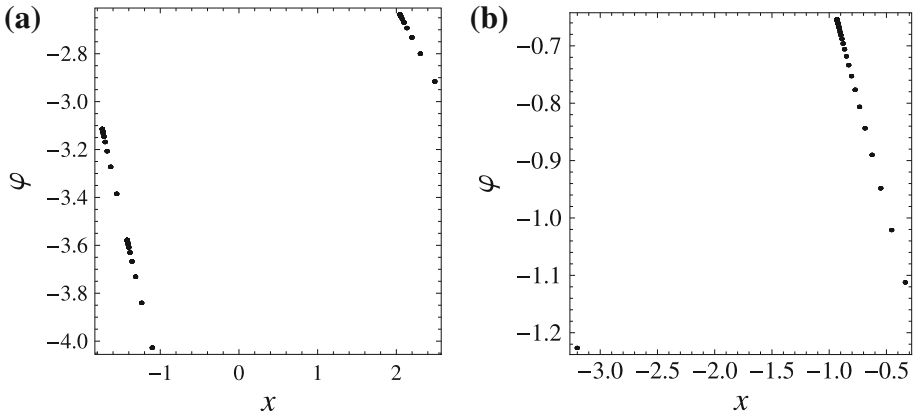

Fig. 11 Poincaré sections of two multi-periodic orbits for $\overline{\mu}_0 = 23.0580008$ (**a**) and $\overline{\mu}_0 = 24.819906$ (**b**)

black diagram for $\varepsilon_{\lambda_s} = 10^{-7}$. Since one cannot observe gray color, we can conclude that diagrams are almost identical and the values of the parameter ε_{λ_s} used in the simulations are sufficiently small.

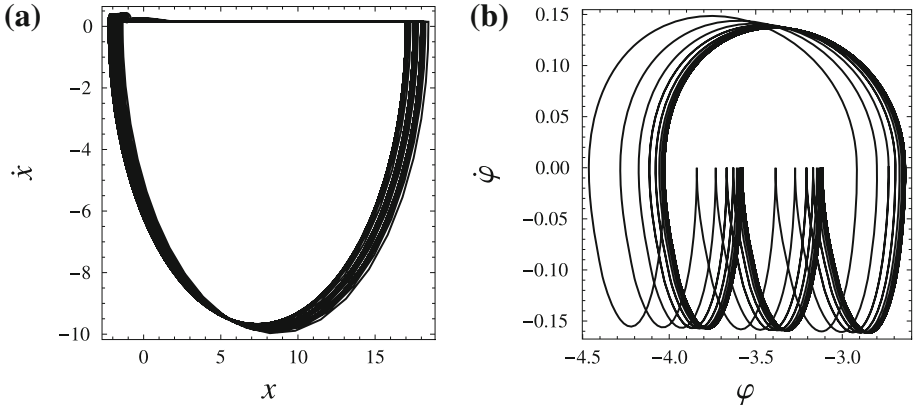

Fig. 12 Multi-periodic orbit for $\overline{\mu}_0 = 23.0580008$

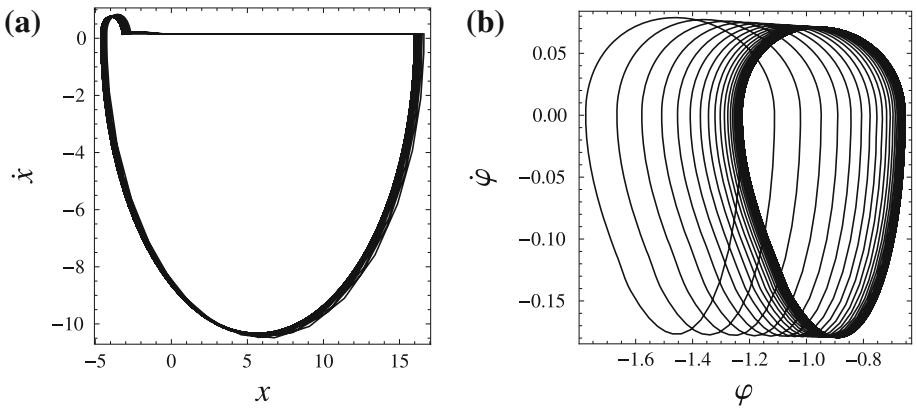

Fig. 13 Multi-periodic orbit for $\overline{\mu}_0 = 24.819906$

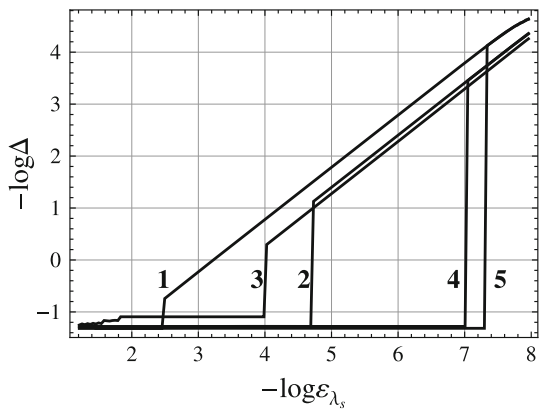

Fig. 14 Error of the solution Δ as a function of the parameter ε_{λ_s} for the following values of the static friction coefficient: $\overline{\mu}_0 = 24.9$ (1), $\overline{\mu}_0 = 23.06$ (2), $\overline{\mu}_0 = 13.5$ (3), $\overline{\mu}_0 = 23.0580008$ (4), $\overline{\mu}_0 = 24.819906$ (5)

Let us note that the concept of small region around the sticking state defined by the small parameter ε_{λ_s} is rather a part of the dynamical system than a property of numerical method. Similarly, the solution concept presented in the previous section defines completely new dynamical system rather than a solution method to a certain differential equations with set-valued functions. The well known problems with the solution uniqueness in the mechanical systems with the so-called stiction friction model (the static friction coefficient is greater than the dynamic one) not necessary take a place in our case. The developed system can be, in certain sense, understood as some kind of switching system with approximation of sticking region [13]. The best test for the method would be the real experiment.

Concluding Remarks

In the paper an original problem of modeling and numerical analysis of system with two-dimensional stick-slip phenomenon has been undertaken. The developed hybrid event-driven model along with the corresponding numerical simulation algorithm allows for effective numerical analysis of the system by the use of standard ODEs integrators.

Few original generalizations of the functions approximating the exact integral model have been proposed. One of them, i.e. Padé approximant lead to special cases presented in other works [7–9]. The extension of the Padé functions to irrational ones of the form [24,25] can improve the approximation, since the elliptic curve is described by the functions of this class and the boundary of the set of admissible values of the friction components is of the elliptic-like shape. Making use of the property (29) of the integral model can lead to further improvement of the approximation. However it is not obvious which of the approximants is most effective since the real normal stress distribution as well as real friction phenomenon are burden with uncertainties. Then the coefficients of the approximate models can be estimated from experimental data instead of fulfilling certain properties of the integral models. From the above reasons we have assumed the simplest approximation (23) of the full integral model in the presented numerical simulations.

As shown in the previous section, the investigated system for some parameter sets can exhibit very rich bifurcational dynamics with self-excited stick-slip motions of very long periods. On the fractal-like bifurcational diagram we can observe many repeating period-adding scenarios and each of them seems to contain the same scenarios of the period-adding phenomenon. Non-periodic behavior has not been proven numerically on this stage of investigations. However in the same system but with external periodic excitation $F(t) = q\cos\omega t$ we expect both quasi-periodic and chaotic attractors.

While designing the mechanical system, we have tried to exclude lateral forces and displacements of the disk, in order to obtain relatively simple model for the preliminary investigations. There exist however an evident and natural way of further developing of the system. First of all we can add one lateral degree of freedom. Then the lateral forces can be added by special modifications of the elasto-damping connections or by adequate modifications of the normal stress distribution over the contact area. The second one can be obtained taking into account the finite height of the disk or changing the shape of contact (for example elliptic or rectangular). As a result we will deal with a three dimensional friction model (two friction components and friction torque).

Acknowledgments The work has been supported by the Ministry of Science and Higher Education under the grant no. 0040/B/T02/2010/38.

References

1. Awrejcewicz, J., Holicke, M.: Analytical prediction of stick-slip chaos in a double self-excited Duffing-type oscillator. Math. Probl. Eng. Art. No 70245 (2006)
2. Awrejcewicz, J., Olejnik, P.: Friction pair modeling by a 2-DOF system: Numerical and experimental investigations. Int. J. Bifurc. Chaos **15**(6), 1931–1944 (2005)
3. Besselink, B., Van De Wouw, N., Nijmeijer, H.: A semi-analytical study of stick-slip oscillations in drilling systems. J. Comput. Nonlinear Dyn. **6**(2), 021006-1–021006-9 (2011)
4. Huango, G., Yin, G., Dai, G.: Chaotic behavior of a stick slip model for rockburst. Disaster Adv. **3**(4), 526–530 (2010)
5. Kang, J., Krousgrill, C.M.: The onset of friction-induced vibration and spragging. J. Sound Vib. **329**(17), 3537–3549 (2010)
6. Contensou, P.: Couplage entre frottement de glissement et de pivotement dans la téorie de la toupe. Kreiselprobleme Gyrodynamics: IUTAM Symposium, Calerina, pp. 201–216 (1962)
7. Zhuravlev, V.P.: The model of dry friction in the problem of the rolling of rigid bodies. J. Appl. Math. Mech. **62**(5), 705–710 (1998)
8. Zhuravlev, V.P., Kireenkov, A.A.: Padé expansions in the two-dimensional model of Coulomb friction. Mech. Solids **40**(2), 1–10 (2005)
9. Kireenkov, A.A.: Combined model of sliding and rolling friction in dynamics of bodies on a rough plane. Mech. Solids **43**(3), 412–425 (2008)
10. Leine, R.I., Glocker, Ch.: A set-valued force law for spatial Coulomb-Contensou friction. Eur. J. Mech. A Solids **22**(2), 193–216 (2003)
11. Ma, O., Liang, J., Fillmore, S.: A 2D bristle friction force model for contact dynamics simulation. In: ASME dynamic systems and control conference, Hollywood, CA, 2010, pp. 501–508, 2009
12. Acary, V., Brogliato, B.: Numerical Methods for Nonsmooth Dynamical Systems. Applications in Mechanics and Electronics Series: Lecture Notes in Applied and Computational Mechanics, vol. 35. Springer, Heidelberg p 565 (2008)
13. Leine, R.I., Nijmeijer, H.: Dynamics and bifurcations of non-smooth mechanical systems. Springer, Berlin (2004)
14. Bastien, J., Schatzman, M., Lamarque, C.-H.: Study of some rheological models with a finite number of degrees of freedom. Eur. J. Mech. A Solids **19**(2), 277–307 (2000)
15. Janin, O., Lamarque, C.-H.: Comparison of several numerical methods for mechanical systems with impacts. Int. J. Numer. Methods Eng. **51**(9), 1101–1132 (2001)
16. Awrejcewicz, J., Supeł, B., Lamarque, C.-H., Kudra, G., Wasilewski, G., Olejnik, P.: Numerical and experimental study of regular and chaotic motion of triple physical pendulum. Int. J. Bifurc. Chaos **18**(10), 2883–2915 (2008)
17. Awrejcewicz, J., Kudra, G.: Modeling, numerical analysis and application of triple physical pendulum with rigid limiters of motion. Arch. Appl. Mech. **74**(11–12), 746–753 (2005)
18. Glocker, Ch.: Formulation of spatial contact situations in rigid multibody systems. Comput. Methods Appl. Mech. Eng. **177**, 199–214 (1999)
19. Pfeiffer, F., Glocker, Ch.: Multibody dynamics with unilateral contacts. Wiley, New York (1996)
20. Awrejcewicz, J., Lamarque, C.-H.: Bifurcation and chaos in nonsmooth mechanical systems. World Scientific, Singapore (2003)
21. Moreau, J.J.: Unilateral contact and dry friction in finite freedom dynamics. In: Moreau, J.J., Panagiotopoulos, P. (eds.) Non-Smooth Mechanics and Applications, pp. 1–82. Springer, Wien (1988)
22. Stewart, D.E., Trinkle, J.C.: An implicit time-stepping scheme for rigid body dynamics with inelastic collisions and Coulomb friction. Int. J. Numer. Methods Eng. **39**(15), 2673–2691 (1996)
23. Möller, M., Leine, R. I., Glocker, Ch.: An efficient approximation of orthotropic set-valued force laws of normal cone type. In: Proceedings of the 7th EUROMECH solid mechanics conference, Lisbon, Portugal, 2009
24. Andrianov, I.V.: Application of Padé-approximants in perturbation methods. Adv. Mech. **14**(2), 3–25 (1991)
25. Andrianov, I.V., Awrejcewicz, J.: New trends in asymptotic approaches: summation and interpolation methods. Appl. Mech. Rev. **54**(1), 69–92 (2001)